ELSEVIER

Cement & Concrete Composites 23 (2001) 227–236

Cement & Concrete Composites

www.elsevier.com/locate/cemconcomp

Image analysis of 'natural' concrete samples by automated and manual procedures

P. Stroeven [a,*], A.P. Stroeven [b], D.H. Dalhuisen [a]

[a] *Faculty of Civil Engineering and Geosciences, Delft University of Technology, Stevinweg 4, 2628 Delft, Netherlands*
[b] *Department of Quaternary Research, Stockholm University, 106 91 Stockholm, Sweden*

Abstract

Nature provide deposits with a structure and properties resembling those of man-made concrete. A tillite at Mt. Feather, McMurdo Dry Valleys, Transantarctic Mountains, Antarctica, is such a deposit. This ancient glacial deposit is of considerable importance to the early glacial history of the Antarctic Ice Sheet. The power of stereological analysis for an objective determination of the preferred direction of small clasts ($\leqslant$5 mm) was investigated in sediment samples from this deposit. Orthogonal sets of vertical thin sections were therefore subjected to a directed secants analysis. The operations were executed in an automated set-up and manually. The roses of intersections were analysed for preferred orientation, the results of which were combined to yield the tilt angle of the clasts. The preferred orientation signal is weak. As a result, in the automated set-up this signal is camouflaged by the effect of digitisation, hampering the assessment of a reliable estimate for the preferred orientation. The manual procedure, although basically more time-consuming, is more accurate and should be preferred, especially in the case of weak signal characterisation, as met in the present situation.

Keywords: 'Natural' concrete; Tillite fabric; Orientation analysis; Line scanning; Roses of intersections; Tilt angle of clasts; Antarctica; Sirius Group

1. Introduction

Tills and tillites, like concrete, are particulate composites of which the mechanical properties are related to the structure and the composition of the material. By one definition, tills are sediments deposited directly by a glacier without reworking by meltwater. Such sediments are often unconsolidated, unsorted and unstratified. Tillites are sedimentary rocks formed of lithified till, including hardening by cementation and induration, and, in essence, have mechanical properties and reveal structural features (Fig. 1) as if they were a 'natural' form of concrete. However, there is still a wide measure of disagreement on the definition of these terms [1].

The spatial organisation of particles in the fine-grained clayey tillite matrix, i.e., till fabric, is of more interest to geologists than from a purely geotechnical point of view only. This is because elongated particles are expected to assume a preferred direction of orientation that relates to the direction of glacier flow. Elongated clasts within the ice body assume a position with their long axes parallel to the direction of ice flow [2]. Commonly that fabric is preserved or reinforced upon deposition when rearrangement of clasts and smaller particles around and in between these clasts is dictated by the pressure field imposed by the overriding ice body. In short, the long axes of particles are observed to predominantly align parallel to the direction of ice flow (in plan view), presumably along shear planes or micro-foliation structures [3,4], although transverse alignment can locally be important [5]. Long axes are found to dip towards the up-glacier direction when deposited on flat and horizontal terrain [6].

Macro-fabric analysis, i.e., of the three-dimensional orientation of large and elongated clasts, is therefore the traditional technique of establishing former ice flow directions in the field [2,7,8]. This method, though widely used for reconstructions in low-relief terrain, is prone to operator dependent decisions on clast suitability [9,10]. This problem can be largely neglected when large numbers of clasts are analysed, but this makes the procedure time-consuming and laborious.

A potentially more convenient means of establishing former directions of ice flow is by micro-fabric analysis

* Corresponding author. Tel.: +31-015-278-4035; fax: +31-015-261-1465.
E-mail address: p.stroeven@ct.tudelft.nl (P. Stroeven).

0958-9465/01/$ - see front matter
PII: S0958-9465(00)00064-0

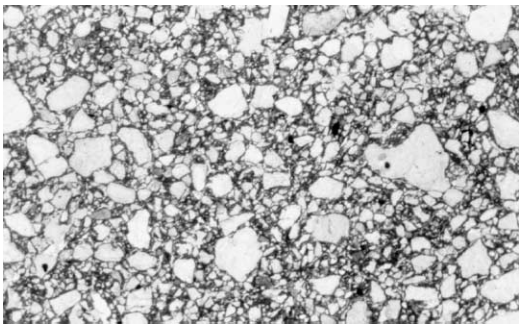

Fig. 1. Example of an analysed image of a 35 mm wide thin section of a tillite sample, revealing a striking similarity with concrete.

in a laboratory environment on thin sections prepared from sediment cores. The most common sectioning technique involves two or three mutually perpendicular sections of which one is used to measure long-axis orientation in the horizontal (bearing) and the other(s) to measure long-axis orientation in the vertical (plunge) [5,11]. The principal shortcoming of the technique (that the analysis of clasts is essentially two-dimensional, i.e., observations in planes) [12] is that the true three-dimensional shape of grains cannot be determined because parts of the grains were ground off [13].

An alternative, previously unexplored, objective method to determine the micro-fabric of tills in three dimensions is to make use of traditional stereological techniques such as the analysis by total projections or line scanning [14]. Stroeven et al. [15] applied this technique to core sample C337 from the Sirius Group tillite on Mt. Feather, Transantarctic Mountains, Antarctica [16–18] to illustrate how the preferential direction of sand particles could be derived in an automated, objective, and cost-effective manner. However, because the orientation of the core sample relative to magnetic north was unknown, only the strength of the preferred orientation direction of micro-clasts could be determined, not the former direction of ice flow.

Stroeven et al. [15] found that the partial orientation signal was quite weak. Hence, we expected that the roses would reveal a slightly oval (or ellipsoidal) shape, with one of the principal axes oriented in the direction of preferred orientation of the particle sections in the image plane. However, the roses of intersections obtained by the method of directed secants showed flower-like shapes, reflecting a dominant effect of digitisation on the image pattern. This seriously hampered the precise and direct assessment of the orientation of the principal axes [15]. Samples C337 and C338 (cf. [19] for parent publication in which sample characteristics are detailed and for description of sample preparation techniques) were therefore also subjected to a manual analysis, the results of which were submitted recently. Here, we will primarily concentrate on a methodological comparison between the stereological approaches to analogue and digitised images. Automatic image analysis operations can be executed in a relatively expeditious and objective way. However, we show that in cases where the particle structure only reveals a relatively weak fabric, the manual procedure will lead to a more reliable estimate. This will equally hold for problems in concrete technology, of course.

2. Modelling of clasts

The tillite from which the actual core samples were drawn is simulated by a two-phase system, consisting of a uniform matrix and dispersed non-spherical particles. Although not essential for the experimental assessment of the preferred orientation direction of the clasts, for visualisation purposes the particles can be assumed oblong (primarily extending – elongated – in one direction), or oblate (primarily extending – elongated – in two directions). For a system of dispersed *oblong particles* with a preferred orientation, the *orientation axis*, l, and the $\{x,y\}$-plane of a Cartesian co-ordinate system $\{x,y,z\}$ enclose an angle α (Fig. 2). Hence, a plane exists, which contains both the z-axis and l. An orthogonal co-ordinate system $\{s,z\}$ is located in this plane. Π is a plane through l perpendicular to the $\{s,z\}$-plane. The Π- and $\{x,y\}$-planes intersect along the line m.

Similarly, an *orientation plane*, Π, can be defined in case of a system of dispersed *oblate particles*. This plane also encloses the angle α with the $\{x,y\}$-plane. So, both types of particles lead to a similar situation. The $\{x,y\}$-plane is called the *horizontal* plane, because it approximately corresponds to a plane perpendicular to the earth's radius at the original core location. The angle α can therefore be associated with the *inclination* or *tilt* of the small clasts.

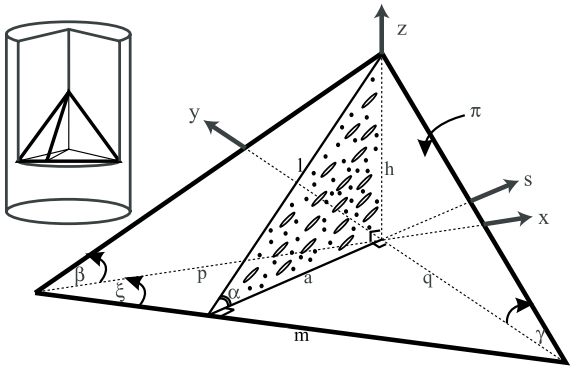

Fig. 2. Assessment of the tilt angle, α, in a tillite matrix by line scanning of an orthogonal set of vertical sections yielding information on the preferred orientation angles, β in the the $\{x,z\}$-plane, and γ in the $\{y,z\}$-plane.

The orientation in space of individual particles will fluctuate around the average situation, as depicted by Fig. 2. Actual deviations from this situation can be expressed in two independent angular parameters of a stochastic nature, and with average values equal to zero.

3. Assessment of tilt angle

Two arbitrary but mutually orthogonal vertical sections, used for the investigations, are defined by the $\{x,z\}$-plane and the $\{y,z\}$-plane, respectively. The $\{y,z\}$-plane and the $\{s,z\}$-plane enclose an angle ξ. Photographs of (part of) the image planes were subjected to a sweeping line scanning operation (a directed secants analysis) for the construction of roses of intersections. This allows determination of the respective angles of preferred orientation in the plane, β and γ (Fig. 2). Herewith, the following relationships are readily obtained:

$$\sin\xi = \frac{a}{p}, \tag{1}$$

$$\cos\xi = \frac{a}{q}, \tag{2}$$

$$\tan\beta = \frac{h}{p}, \tag{3}$$

$$\tan\gamma = \frac{h}{q}, \tag{4}$$

$$\tan\alpha = \frac{h}{a}. \tag{5}$$

By combining Eqs. (1) and (2), it is found that

$$\sin^2\xi + \cos^2\xi = a^2\left(\frac{1}{p^2} + \frac{1}{q^2}\right). \tag{6}$$

Upon substitution of Eqs. (3)–(5), this yields

$$\tan^2\alpha = \tan^2\beta + \tan^2\gamma. \tag{7}$$

In summary, two vertical sections of a sample from both cores were analysed by sweeping test lines to determine the roses of the number of intersections of the test lines with the perimeter traces of the dispersed small clasts. The rotation angle of the roses define the respective apparent orientation angle (β and γ). The tilt angle, α, is obtained upon substitution in Eq. (7).

4. Orientation analysis by line scanning

Orientation analysis by line scanning involves coverage of the image plane by a grid of parallel lines, the so called *directed secants*, whereupon the number of intersections with the *traces* of the particle surfaces are counted [20]. The number of intersections is indicated by P, and the intersection density by $P/L = P_L$, where L is the total line length of the grid. Perpendicular to the orientation axis of the traces the intersection density will have a maximum, while a minimum is found parallel to the orientation axis. It is well known that the intersection density in a certain direction, $P_L(\theta)$ will equal the total projected length of the traces (L') per unit of area (A), on a line perpendicular to the grid direction, $L'_A(\theta + (\pi/2))$ [20]. Hence,

$$P_L(\theta) = L'_A\left(\theta + \frac{\pi}{2}\right). \tag{8}$$

For the two-dimensional case, it is assumed that the actual trace system can be approximated by a mixture of random and oriented line segments, respectively L_r and L_o. L_o is considerably smaller than L_r in the case of our materials. By dividing by the sampled area, A, the appropriate line densities are obtained. According to Eq. (8), the line segments are 'measured' in proportion to their total projected length perpendicular to the line array. This allows for the construction of a rose of intersections for a system of random and oriented line segments in a vertical plane, of which the latter enclose an angle $\beta + (\pi/2)$ with the horizontal (say, x-) axis. This type of approach has been applied in concrete technology to analyse crack density and orientation [21,22]. In the case of the digitised image, all line segments building up the particle's perimeter in the section plane are replaced by their total projections in the x- and y-directions. Hence, this system is composed of two oriented portions enclosing an angle of $\pi/2$. Note that in the automated and manual approaches it was not pursued to estimate L_A or even S_V (specific surface area of clasts), so that data recording can be restricted to intersection counts (P) only.

4.1. Rose for partially oriented system of line segments in a plane (manual model)

The contours of the particles are smooth in the analogue picture subjected to the manual orientation analysis. It is assumed that in the orthogonal pair of vertical sections these perimeter traces can be conceived as a mixture of two-dimensional randomly oriented segments and oriented ones. The treatment is similar for these two vertical sections, so that the discussion can be restricted to the $\{x,z\}$-plane only.

The number of intersections per unit of line length is on average a constant for the random portion of line segments, say P_{L_r}. The oriented portion reveals a maximum value, P_{L_o}, perpendicular to the direction of preferred orientation, in a direction enclosing an angle β with the x-axis. This value will decline when the line system is rotated over an angle θ to $P_{L_o}\cos\theta$. These two components are combined in Fig. 3 (cf. [20, Fig. 3.8]). The large circle, with radius P_{L_r} represents the random

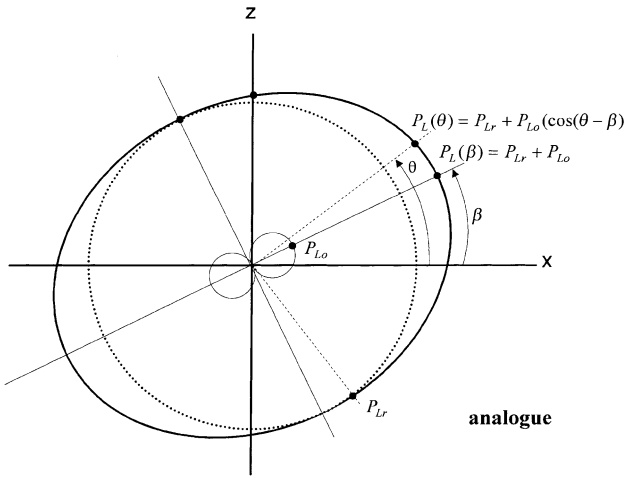

Fig. 3. Rose of intersections for a combination of random and oriented line segments in a plane (manual model). In the presented case, x is the horizontal and z the vertical axis, and β the angle of preferred orientation. The same solution pertains to the $\{y,z\}$-system in the other vertical section, whereby β should be replaced by γ.

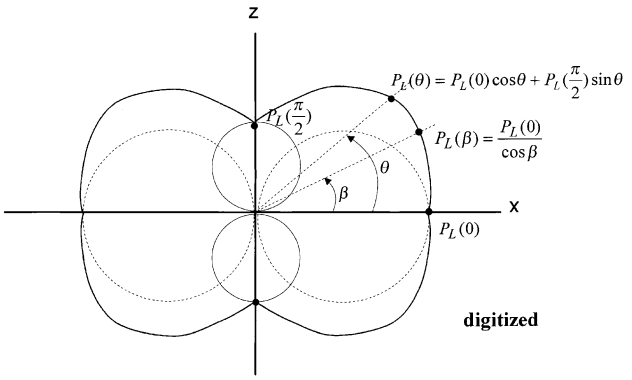

Fig. 4. Roses of intersections for an orthogonal set of oriented line segments (automated model). In the presented case, x is the horizontal and z the vertical axis, and β the angle of preferred orientation. The same solution pertains to the $\{y,z\}$-system in the other vertical section, whereby β should be replaced by γ. Note that P_L is given for the first quadrant.

portion. The two smaller circles pass through the origin, have a diameter P_{L_o}, while the line through their centres (and the origin) encloses an angle β with the x-axis. Hence, for a line system enclosing an angle θ with the x-axis, $P_L(\theta)$ would be given by

$$P_L(\theta) = P_{L_r} + P_{L_o}\cos(\theta - \beta). \tag{9}$$

This rose has its maximum value of $P_L(\theta)$ for $\theta = \beta$. Hence, $P_{L\max} = P_{L_r} + P_{L_o}$.

Note that the relationships derived for intersection densities will also hold for the number of intersections when L is a constant (as in our investigations).

4.2. Rose for mixture of orthogonal systems of line segments in a plane (automated model)

The perimeter contours in the digitised images, corresponding to the orthogonal pair of vertical sections, are composed of orthogonal line segments due to digitisation in 4-connexity. They are oriented in either the x- and z-directions, or in the y- and z-directions, respectively. The treatment is similar for these two sections, so that the discussion can be restricted to the $\{x,z\}$-plane only.

The oriented portions are represented by circles passing through the origin and oriented in x- and z-directions, respectively (Fig. 4). The diameter of the vertical pair of circles is denoted by $P_L(\pi/2)$, whereas the diameter of the horizontal pair of circles is $P_L(0)$. Since $P_L(\theta) = P_L(0)|\cos\theta| + P_L(\pi/2)|\sin\theta|$, it can be derived that $P_L(\theta)$ will have its maximum value for $\tan\beta = P_L(\pi/2)/P_L(0)$. Upon substitution, the expression for intersection density in an arbitrary direction θ is found

$$P_L(\theta) = \frac{P_L(0)}{\cos\beta}|\cos(\beta - \theta)|. \tag{10}$$

A comparison of Eqs. (9) and (10) learns that the two representations of the *same image* are different on important aspects. This is also reflected by the roses of Figs. 3 and 4. Fig. 3 is symmetric around an orthogonal system of axes, inclined by an angle β with the x-axis. Fig. 4 is symmetric around the x- and the z-axes (cf. [20, Fig. 3.3 (b-2)]). In Fig. 3, the shape of the curve in the two successive quadrants is different; in Fig. 4 they are similar, with the crucial consequence of not being able to determine whether the preferred orientation of the clasts is in a direction β or in a direction $\pi - \beta$! Selection of the proper solution among these two options should be based on insight into the technical problem. Basically, in both situations the angle β can be obtained by fitting a cosine function to the data set. Note that the relationships derived for intersection densities will also hold for the number of intersections when L is a constant (as in our investigations).

5. Image analysis of samples

5.1. Automatic procedure

Images of sub-areas with a size of 36×24 mm^2 were available for the analysis. Each vertical section provided 14 of such areas, with two orthogonal sections per core. For further elaboration, the scanned (digitised) images (at 820×520 pp resolution) were employed. Some of the images reveal disturbed areas due to outer edges of the core or of the thin section. Some also have relatively large 'cracked' zones. Therefore, a defect-free 340×340 pp square area of analysis was applied to 13 out of 14

available slides per section. All field images with linear dimensions of about 15 mm were subjected to a software-driven filtering operation, leading to a particulate structure from which the fines were removed. Fig. 5 shows one example of an image from a sub-area (of which contrast is somewhat improved), and the selected field. The fields were subjected to the directed secants analysis. All particle sections having the tangent point with a horizontal line at the bottom side of its perimeter outside the field were omitted from the orientation analysis. Fig. 6 presents a rose of the number of intersections obtained in this way. Note that the rose's radius does not start at zero, so differences are exaggerated. The roses pertaining to the 13 images of one vertical section of a core sample were combined for the construction of an 'average' rose being more representative for the underlying material structure. The amount of scatter was reduced as a result in these roses.

5.2. Manual procedure

The 36×24 mm^2 slides of the thin sections were projected (with a magnification of about $20\times$) on a semi-transparent screen and manually copied. Only sand-sized particles in the section image were admitted, as can be observed from Fig. 7, presenting the hand-copied field image TR302. These field images were subjected manually to a directed secants analysis by superimposing a grid engraved on a circular Perspex plate of 300 mm diameter. The grid consisted of equidistant grid lines 10 mm apart. This line spacing (at least) fulfilled the rule of thumb that optimum conditions are achieved

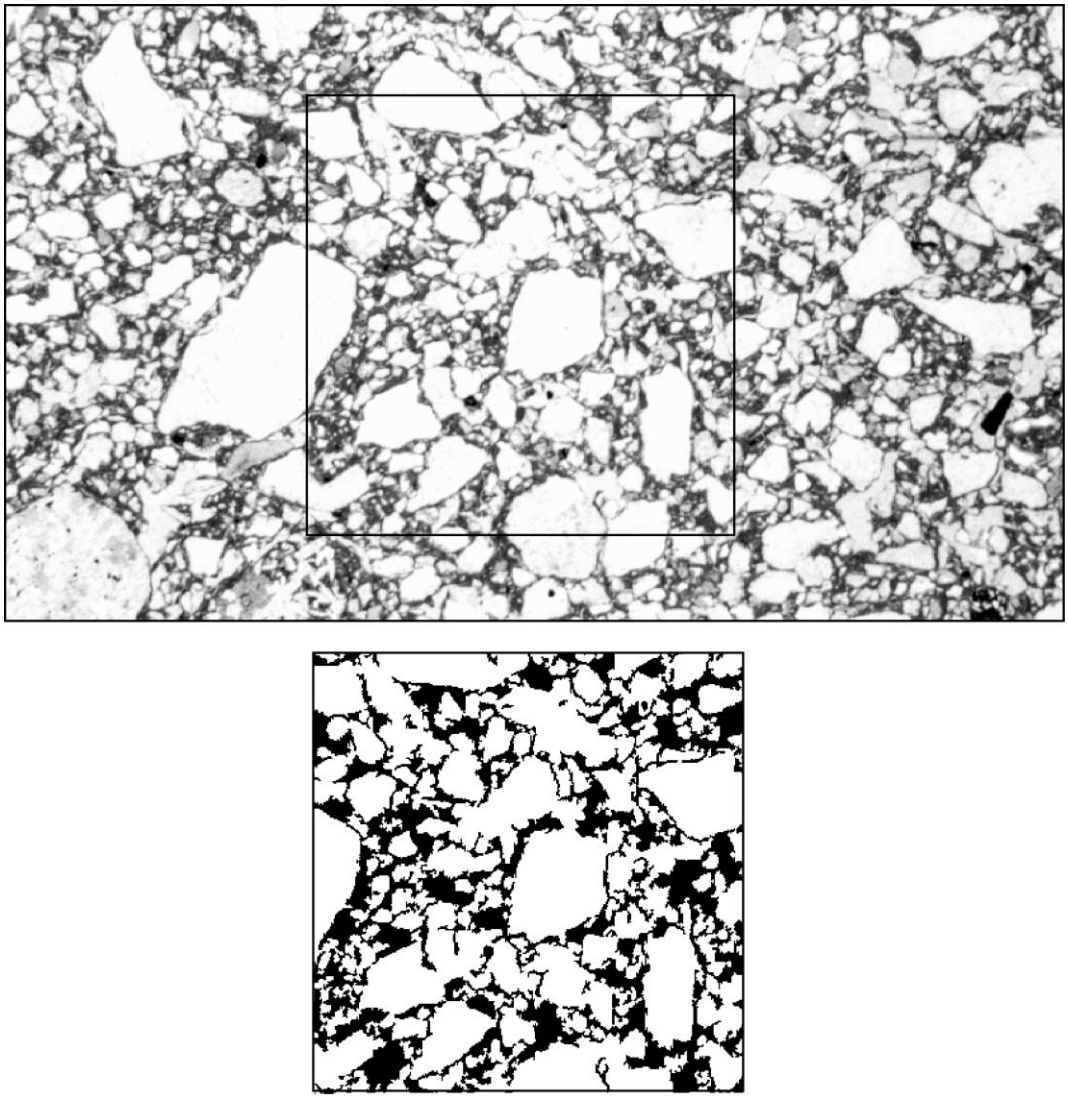

Fig. 5. Image of a 35 mm wide thin section coded TR203 with the core axis in vertical direction, representing a major part of the slide (24×36 mm^2). The field subjected to automatic systematic line scanning is indicated at the bottom (about 15×15 mm^2).

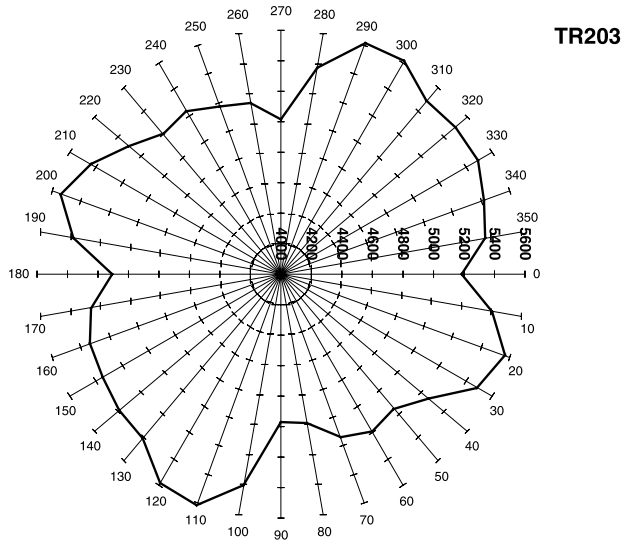

Fig. 6. Rose of intersections of single field obtained by automatic systematic line scanning. Note that the radial co-ordinate starts at 4000.

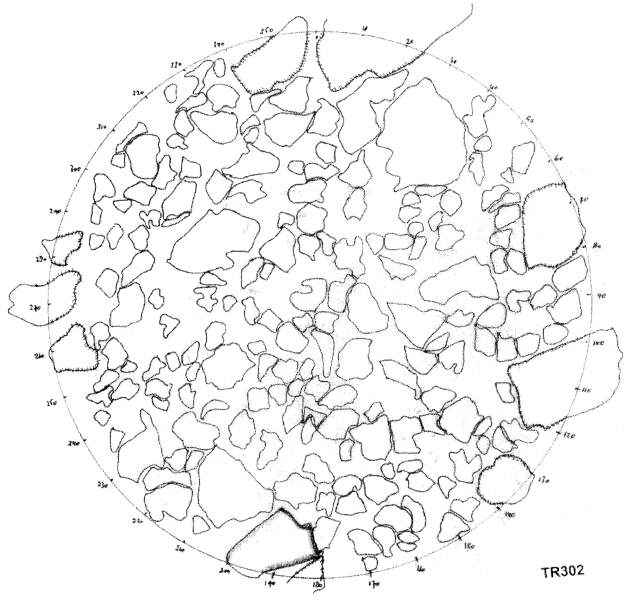

Fig. 7. Field image obtained by a manual copying process. The same area is indicated in Fig. 8.

when the number of particle intercepts (which is half the number of intersections) correspond to the number of particle sections in the image plane. A higher line density would lead to recurrent information. An example of a rose of a single field is presented in Fig. 8. As in the case of the automatic analysis, the 13 roses pertaining to a vertical section were combined (in this case added) for the construction of the corresponding rose of the number of intersections representing a vertical section. The vertical sections of core sample C337 were analysed in this way.

6. Results

In all cases, roses pertaining to a particular vertical section were combined to yield an average (automated procedure) or total (manual procedure) rose of intersections. The roses corresponding to the four vertical sections obtained by the automated image analysis procedure are presented in Fig. 9. The flower-like shapes of the roses are in agreement with the automated model displayed in Fig. 4. The 15 mm square field image of TR203 shown in Fig. 10 at a somewhat larger magnification, indeed reflects the perimeters of particle sections to be replaced by horizontal and vertical line sets only, due to the digitisation process in 4-connexity.

The total roses obtained by the manual procedure of image analysis clearly reveal a direction of preferred orientation (cf. Fig. 11 for core sample C337). In all cases of manual analysis, the direction of preferred orientation can be determined accurately by means of curve fitting (cf. Fig. 12 for core sample C337). Our analysis of this core sample C337 indicates that the *random signal is about 20 times stronger than the oriented signal*. Further, the two angles β and γ in Eq. (7) are 18° and 32°, respectively. Consequently, by manual procedure the three-dimensional tilt angle, α, can be calculated to approximate 35°.

A similar curve fitting approach was used for the roses obtained by automatic image analysis on sections of the same core sample (Fig. 12). The values for β and γ obtained in this way are 43° and 48°, respectively. To check the underlying model, visualised in Fig. 4, these angles were also determined by other mathematical operations. Upon averaging Eq. (10), an estimate for the angle of preferred orientation is obtained based on *all observations*. It is readily found that

$$\tan\beta = \frac{\pi}{2}\frac{\overline{P_L(\theta)}}{P_L(0)} - 1. \tag{11}$$

Eq. (11) yields values of approximately 45° for β and γ of the vertical sections of core sample C337. This is in agreement with the curve fitting results, considering the effect of natural scatter.

7. Discussion

The sensitivity of the approaches are governed by the size of the field, the grid line density, and the magnification. Optimum density of grid lines (avoiding extra efforts which yield only redundant information) is ob-

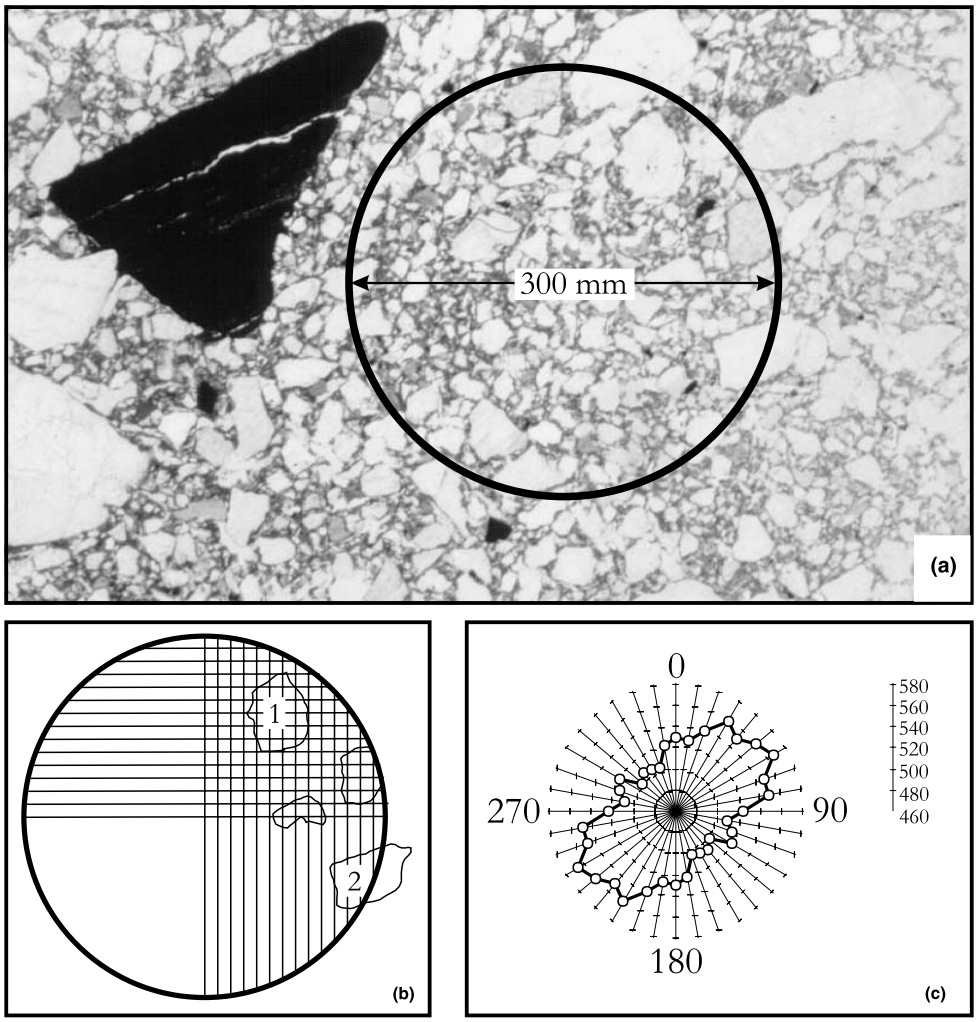

Fig. 8. (a) Image of sub-area TR302 representing a major part of the slide (24×36 mm^2) with the core axis in vertical direction, showing the sampled field of which the hand-copied image is presented in Fig. 7. The field is analysed by manually applying the method of directed secants (b); (c) obtained rose of the number of intersections. Note that the radial co-ordinate starts at 460.

tained when the number of intercepts with particle sections (which is half the number of intersections with their perimeters) would roughly equal the number of particles in the field, N [20,23]. Based on rough estimates for N of 125 and for the volume fraction of particles V_V of 0.5, the coefficient of variation, CV, would be 6% ($\mathrm{CV} = 100\sqrt{(1 - V_V)/N}$). This reduces to 1.5% for the vertical section averages and totals (i.e., a group of 13 roses). Hence, the sensitivity of the approach is quite high, leading to reliable estimates in the manual procedure. In the automated approach, however, the low strength of the oriented signal (i.e., 5% of the total) was insufficient to generate significant differences in the successive directed secants measurements in a wide angular range around the direction of preferred orientation of the particle sections in the vertical plane. A larger magnification would allow for a better representation after digitisation of the particle contours. A further improvement can be expected by 6-, or 8- instead of 4-connexity lattices in the digitisation process. Such facilities were not available in our case. In both approaches, curve fitting is the proper way in estimating the angle of preferred orientation.

A comparison between the shapes of the average and total roses, following either from the automated or from the manual procedure, respectively, reveals that the signal in the case of the automated procedure is camouflaged by the digitisation effect on the magnification level selected for these investigations; this is a well-known phenomenon [24]. It can be quantified by separating in 4.2 the projections in x- and z-directions of the random and of the oriented signals. As a result, Eq. (10) is transferred into

$$P_L(\theta) = \sqrt{2}P_{L_r}\left|\cos\left(\theta - \frac{\pi}{4}\right)\right| + P_{L_o}|\cos(\beta - \theta)|. \qquad (12)$$

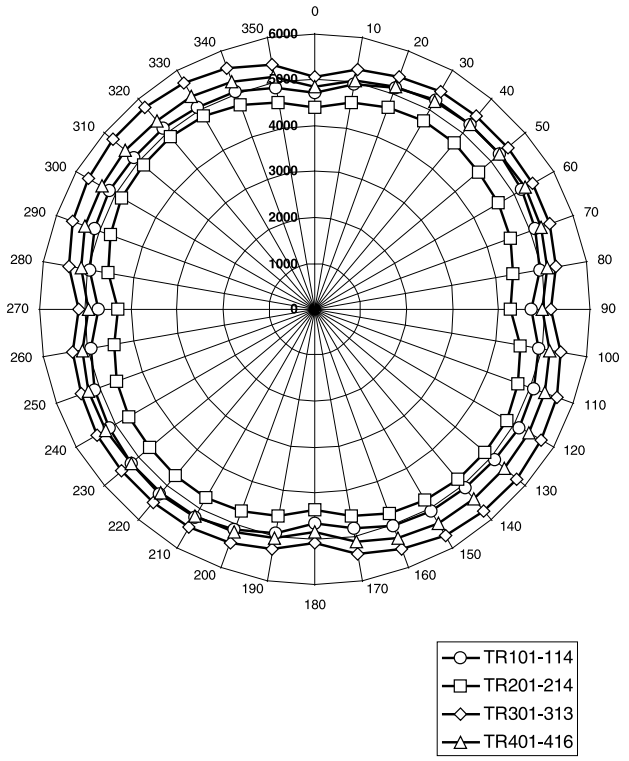

Fig. 9. Average roses of intersections obtained by automated systematic line scanning of 13 fields from TR101-114 and TR301-313, respectively representing the two vertical sections of core C337, and of the 13 fields from TR201-214 and TR401-416, respectively representing the two vertical sections of core C338.

This function has its maximum value for $dP_L(\theta)/d\theta = 0$, yielding the equality

$$\sqrt{2}P_{L_r}\sin\left(\theta-\frac{\pi}{4}\right)+P_{L_o}\sin(\theta-\beta)=0. \tag{13}$$

Eq. (13) demonstrates that for weak signals, the maximum in the curve will shift to $\theta = \pi/4$ (governed by the digitisation effect), as was indicated earlier [15]. Only when $P_{L_o} \gg P_{L_r}$, the maximum can be associated in a reliable way with the angle of preferred orientation, β. This also holds for an expression like Eq. (11). Hence for relatively weak signals, only the manual approach can straightforwardly yield reliable estimates. Such weak signal can be an inherent property, such as in the case of the tillite material. As argued earlier, selecting a higher magnification and more complicated lattice systems for digitisation could have yielded somewhat better results. Fig. 10 gives a qualitative impression of the choice on the magnification level.

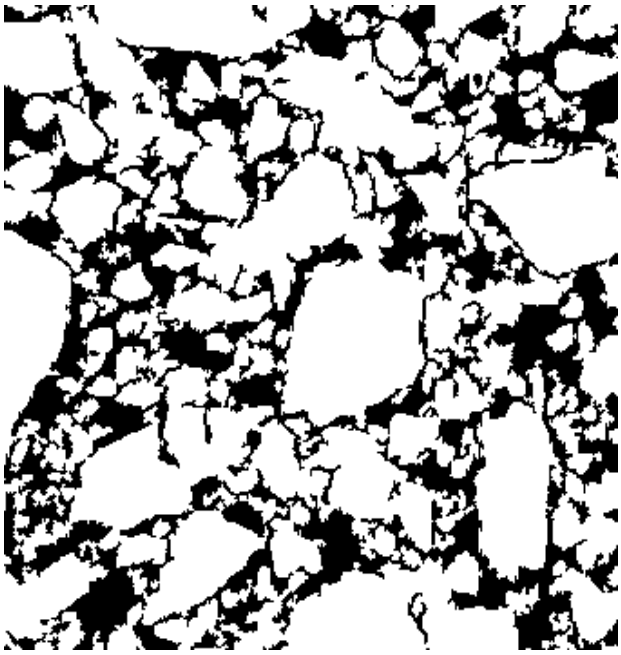

Fig. 10. Due to the digitisation process, the pixelation introduces bias in the geometry of the 'contours' of the particles. As a result, such contours are only composed of two orthogonal sets of line segments in the case of a 4-connexity lattice, as demonstrated by the 15 mm square field image TR203 also presented in Fig. 5.

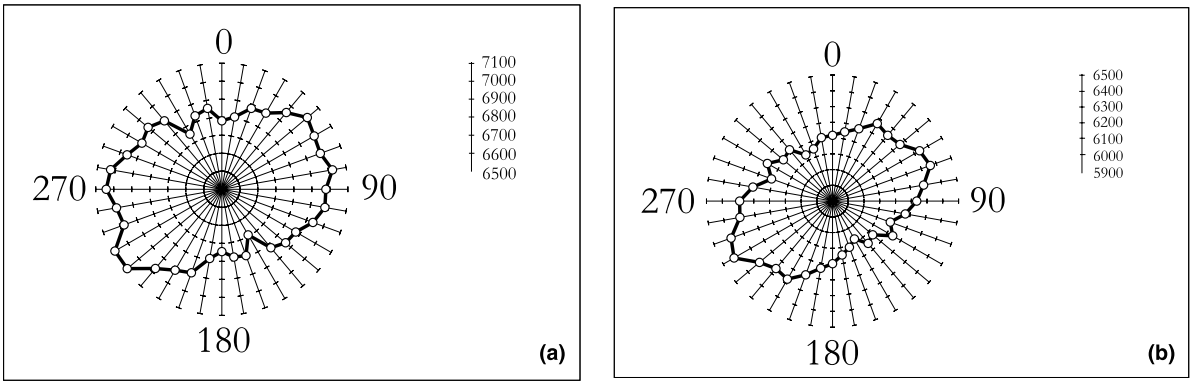

Fig. 11. Total roses of intersections pertaining to the orthogonal set of vertical sections of core C337 obtained by manual application of the method of directed secants. (a) TR101-113 (radial co-ordinate starts at 6500) and (b) TR301-313 (radial co-ordinate starts at 5900).

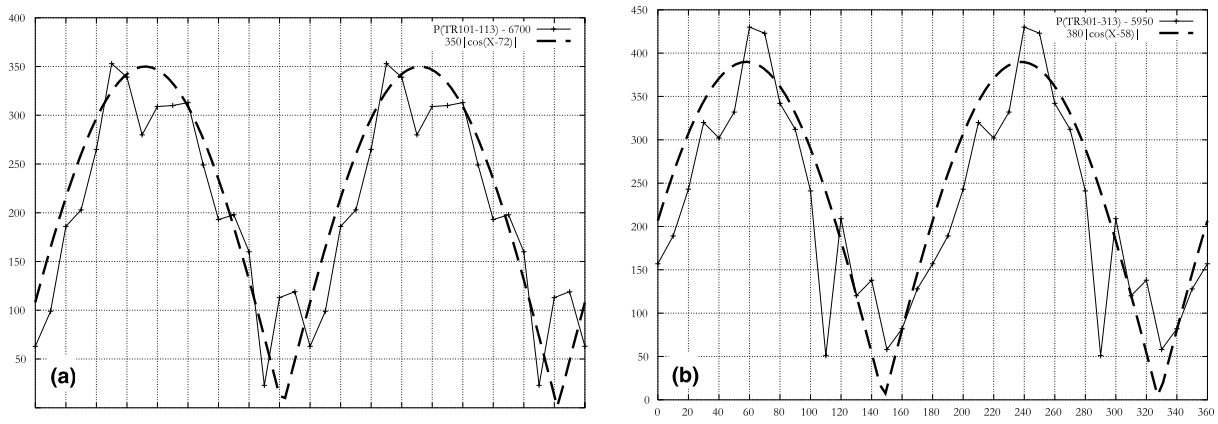

Fig. 12. The reduced signals of Fig. 11, i.e., ($P_{\mathrm{TR101\text{-}113}} - 6700$) (a), and ($P_{\mathrm{TR301\text{-}313}} - 5950$) (b), are approximated by a cosine curve fitting operation.

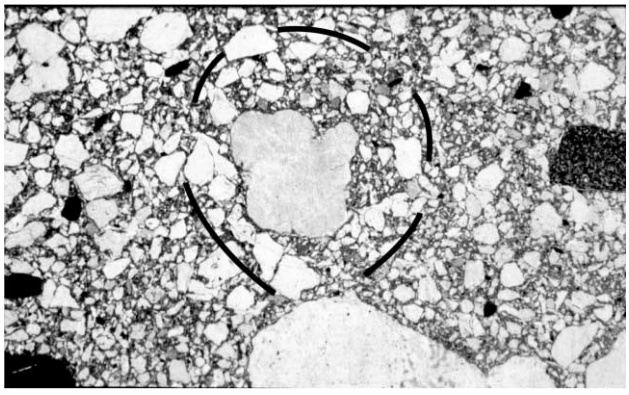

Fig. 13. Turbate structure visible in thin section of vertical section of a core sample.

The vertical component of the preferred orientation, α, when governed by deposition (lodgement) at the base of the glacier without subsequent deformation, would attain a value close to zero (horizontal). However, the average preferred vertical orientation of the measured particles by manual and by automatic procedures deviates significantly from zero, and is, therefore, inconsistent with till lodgement without post-depositional deformation. Deformation in the till probably occurred along discrete shear planes or within widening shear bands (due to dilatancy processes). If so, we have obtained a measure of the dominant direction of these shear planes. It reflects, primarily, the structure and composition of the till under the loading exerted by the overlying ice.

Micro-morphological observations by van der Meer et al. [19] on the thin sections on which this paper is based yielded that the till was subjected to post-depositional sub-glacial deformation (i.e., resulting in turbate deformation structures of matrix grains; Fig. 13). Hence, the observed micro-fabric by manual and automated procedures encompasses the influence of these turbate or rotational structures typical for wet-based sub-glacial tills [25]. Nevertheless, turbate structures cannot dominate the orientation of elongated grains in our thin sections because if they did, a clear signal of the preferred orientation of particles would not be, a priori, expected. However, because the preferred orientation direction of small particles in lodgement tills is actively dictated by the flow direction of the overlying ice (and is not an inherited signal), we conclude that the influence of turbate structures on the totalled micro-fabric is a measurable signal in the transverse (although we cannot exclude other influences such as a high percentage of rod-shaped particles, for which a position transverse to the ice flow direction is energetically favourable).

8. Conclusion

The presented stereological approach to three-dimensional orientation analysis for determination of the tilt angle of small clasts in Antarctic tillite is *objective and exact*, and can be automated. A similar approach is possible, of course, in case of man-made concrete where a preferred orientation of particles may originate from a particular compaction technique, or where crack orientation is of interest [22,23]. In contrast, the commonly employed method of fabric or orientation analysis in tills and in concrete technology [26] consists of classification of the orientation of individual particles or particle sections, a time-consuming and subjective process.

An accurate estimate of the direction of the main axes of the rose of intersections is derived by the method of directed secants, even when analysing weak orientation signals as in the present problem. Determination by manual procedure on analogue images results in a straightforward analysis, when combined with a cosine function curve fitting operation.

The effect of digitisation on roses of intersections of the automatic image analysis hampers the determination

of a reliable estimate for the preferred orientation in the vertical sections. This well-known 'disturbing' effect can be somewhat reduced by subjecting fields of larger magnification to the directed secants analysis and using 6- or 8-connexity digitisation lattices. The automated model for digitised images (Fig. 4) demonstrates that the preferred orientation of the flower-like roses of intersections can be associated with either the direction of preferred orientation of the particles in the vertical section plane, e.g. β, or with the supplemental value, $\pi - \beta$ in case of strong signals only. Under those circumstances, curve fitting by a cosine function can offer a solution to the orientation problem of the clasts, and particles, or of cracks in concrete. For detailed information on possible improvements of this automated approach for orientation analysis, one is referred to the relevant literature [14,24].

References

[1] Hambrey MJ, Harland WB, editors. Earth's pre-pleistocene glacial record. Cambridge: Cambridge University Press; 1981. 1004p.

[2] Holmes CD. Till fabric. Bull Geol Soc Am 1941;52:1299–354.

[3] Glen JW, Donner JJ, West RG. On the mechanism by which stones in till become oriented. Am J Sci 1957;255:194–205.

[4] Evenson EB. The relationship of macro- and microfabric of till and the genesis of glacial landforms in Jefferson County, Wisconsin. In: Goldthwait RP, editor. Till... a Symposium. Ohio State University Press; 1971. p. 345–64.

[5] Johnson MD. The origin and microfabric of Lake Superior red clay. J Sediment Petrol 1983;53:859–73.

[6] Gravenor CP, Meneley WA. Glacial flutings in central and northern Alberta. Am J Sci 1958;256:715–28.

[7] Richter K. Die Bewegungsrichting des Inlandeises rekonstruiert aus den Kritzen und Längsachsen der Geschiebe. Zeitschrift für Geschiebeforschung 1932;8:62–6.

[8] Harrison PW. A clay till fabric: its character and origin. J Geol 1957;65:275–308.

[9] Andrews JT, Smith DI. Statistical analysis of till fabric methodology, local and regional variability. Quart J Geol Soc Lond 1970;125:503–42.

[10] Drake LD. Human factor in till-fabric analysis. Geology 1977;5:180–4.

[11] Evenson EB. A method for 3-dimensional microfabric analysis of tills obtained from exposures or cores. J Sediment Petrol 1970;40:762–4.

[12] Ostry RC, Deane RE. Microfabric analyses of till. Geol Soc Am Bull 1963;74:165–8.

[13] Björnbom S. A method of determining the three-dimensional arrangements of medium sand particles in basal tills and some new facts about these arrangements. Geologiska Föreningens i Stockholm Förhandlingar 1977;99:398–401.

[14] Stoyan D, Beneš V. Anisotropy analysis for particle systems. J Micros 1991;164:159–69.

[15] Stroeven P, Stroeven AP, Dalhuisen DH, van de Meer JJM. Stereological analysis of ice flow-induced preferred orientation of small clasts in Tertiary tillite matrix of Mt Feather. Acta Stereologica 1999;18/1:49–60.

[16] Brady H, McKelvey B. Some aspects of the Cenozoic glaciation of southern Victoria Land, Antarctica. J Glaciol 1983;29:343–9.

[17] Barrett PJ, Bleakley NL, Dickinson WW, Hannah MJ, Harper MA. Distribution of siliceous microfossils on Mount Feather, Antarctica, and the age of the Sirius Group. In: Ricci CA, editor. Geological Evolution and Processes, Siena; 1997. p. 763–70.

[18] Stroeven AP, Kleman J. Age of Sirius Group on Mount Feather, McMurdo Dry Valleys, Antarctica, based on glaciological inferences from the overridden mountain range of Scandinavia. Global Planet Change 1999;23(1–4):231–47.

[19] van der Meer JJM, Hiemstra JF, Stroeven AP. Micromorphology of two Sirius Group core diamict samples from Mt. Feather, Dry Valleys, Antarctica. In: Wilson GS, Barron JA, editors. Mount Feather Sirius Group Core Workshop and Collaborative Sample Analysis, Columbus, OH. USA: The Ohio State University; 1998. p. 96–108.

[20] Underwood EE. Quantitative stereology. Reading, MA: Addison-Wesley; 1970. 274p.

[21] Ringot E. Automatic quantification of microcracks network by stereological method of total projections in mortars and concrete. Cement Concrete Res 1988;18:35–43.

[22] Stroeven P. Geometric probability approach to the examination of microcracking in plain concrete. J Mater Sci 1979;14:1141–51.

[23] Stroeven P. Some aspects of the micromechanics of concrete. PhD Thesis, Delft University of Technology, Delft, 1973, 329p.

[24] Chaix JM, Grillon F. On the rose of directions measurements on the discrete grid of an automatic image analyser. J Micros 1996;184:208–13.

[25] van der Meer JJM. Particle and aggregate mobility in till: microscopic evidence of subglacial processes. Quaternary Sci Rev 1997;16:827–31.

[26] Karl F, Wu M. Gefügeuntersuchungen an Betonen und Discussion des Gefüge-einflusses auf die technischen Eigenschaften. Tonindustrie Zeitung 1970;94(11):449–62.